Hexagonal modulation of two-dimensional HNO_3 clusters in graphite

1989 J. Phys.: Condens. Matter 1 2483

(http://iopscience.iop.org/0953-8984/1/14/004)

J. Phys.: Condens. Matter 1 (1989) 2483–2492. Printed in the UK

Hexagonal modulation of two-dimensional HNO_3 clusters in graphite

J Bremer†, E J Samuelsen† and R Moret‡

† Department of Physics and Mathematics, The Norwegian Institute of Technology, N-7034 Trondheim-NTH, Norway

‡ Laboratoire de Physique des Solides, Université Paris-Sud, F-91405 Orsay, France

Received 2 August 1988, in final form 26 October 1988

Abstract. The in-plane ordering of HNO_3 intercalated in graphite is investigated. Above 248 K the nitrate molecules form a liquid-like phase whose diffraction pattern has been studied in some detail. It is suggested that the intensity distribution is caused by a new type of two-dimensional ordering. The general features of a classical correlation function giving diffuse and hexagonally modulated Bragg spots are outlined. A system of ordered and inhomogeneously contracted clusters of approximate size 600 $Å^2$, consisting of roughly 40–50 scattering centres, is presented as a structural model. The clusters are anchored in such a way that the sixfold symmetry of the correlation function is preserved. Good agreement with experimental data is obtained by allowing for position-dependent fluctuations transverse with respect to a radial lattice contraction. Inter-molecular distances are found to be significantly reduced near the edge of the cluster.

1. Introduction

Graphite intercalation compounds (GICs) are formed when guest molecules or atoms enter regularly spaced carbon layers. In stage n compounds there are n such layers between the two-dimensional dopant structures. During the intercalation process, holes or electrons are injected into the graphite bands, which give rise to changes in conductivity and Fermi level. The materials are highly anisotropic (Lundberg and Sundqvist 1986). They have potential applications in energy storage and catalyst technology. To date, relatively few acceptor intercalants have been studied. The present paper deals with the in-plane structure of nitrate molecules in stage 2 graphite (Fuzellier *et al* 1977) at temperatures above 248 K. In this temperature range, we find that a new, and hitherto unreported, type of structural phase exists.

The scope is as follows: § 2 contains a brief account of the experimental part of the work; in § 3, we present and discuss a classical correlation function which is capable of reproducing observed x-ray scattering data; concrete proposals for the structure together with a discussion will be given in § 4.

2. Experimental details

It is well known that two-dimensionally ordered layers on surfaces are strongly influenced by the substrate structure. A similar situation exists for intercalated materials. The

0953-8984/89/142483 + 10 $02.50

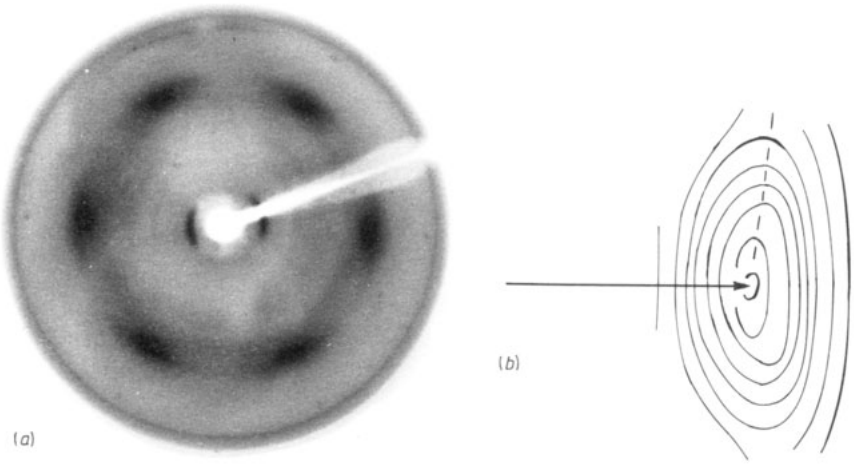

Figure 1. Diffuse spots (see text) from HNO_3 in stage 2 graphite as a function of the two-dimensional scattering vector $Q = (Q_x, Q_y, 0)$. (*a*) X-ray precession photograph showing the spatial variation of intensity at 248 K, just above T_c. The x-ray wavelength λ is 1.5418 Å. (*b*) Smoothed data at $T = 257$ K. At higher temperatures the broadened spots turn into an inhomogeneous ring.

question of the in-plane ordering of HNO_3 molecules at temperatures below 248 K has recently been elucidated. Below 210 K a commensurate superstructure is known to exist. A 'weakly' incommensurate structure was found in the temperature interval between 210 and 248 K (Samuelsen *et al* 1984, 1985). Above 248 K, however, a disordered phase is formed whose diffraction pattern has a hexagonal character. The transition is of first order. The diffraction spots are rotated 30° with respect to the direction of the graphite (100) Bragg maxima and are found at the reciprocal distance $0.37|(110)_G|$ from the origin. These spots are incommensurate with the graphite structure. In addition to being broad, thus indicating a relatively short correlation length, they appear to have a peculiar shape. The angular width is significantly larger for the part of the spot with the largest scattering angle. The overall shape is reproduced in figure 1(*a*). Note that this picture is representative for temperatures close to $T_c = 248$ K. At higher temperatures the six outer rims merge together, taking the shape of a single hexagonally modulated ring. The intensity maxima remain at 30° away from the graphite reflections, but the intensity at the inside of the original smeared HNO_3 spots has vanished.

It is noteworthy that recordings of the type shown in figure 1 are obtained only by using a single crystal, as first found by Samuelsen *et al* (1984, 1985). Recently, we have remeasured the intensity distribution for $T > 248$ K and confirmed the diffraction effect, which—to our knowledge—has not been analysed elsewhere. By means of carefully oriented detector scans at various temperatures the diffuse spots were mapped in some detail. A description of the experimental set-up can be found elsewhere (Samuelsen *et al* 1987).

Figure 1(*b*) represents smoothed data recorded at $T = 257$ K. The broken line shows the location of the maximum intensity. Close to T_c, however, we have effectively only six diffuse spots, and the corresponding molecular arrangement must possess an 'ordered' character. The diffraction pattern resembles, at least qualitatively, the broadened first-order reflections of a small two-dimensional crystal with hexagonal symmetry. The transition to a ring-like intensity distribution occurs gradually with

increasing temperature, as the structure becomes more 'liquid like'. Even at room temperature a weak hexagonal modulation is found to remain.

Domain shape or size effects cannot account for the measured intensity profiles. The reason is that the shape function of a domain will modify all spots in essentially the same manner. This occurs via convolution processes and the spots are thereby given equal symmetry and a relative orientation. The effect is clearly incompatible with the observed gradual transition to an azimuthal intensity distribution. We have checked carefully that the instrumental broadening is negligible. Even if the experimental smearing were non-zero, it could not explain the observed diffraction patterns. The arguments for this conclusion are essentially identical with the above arguments.

According to Halperin and Nelson (1978), continuous melting of two-dimensional crystals may occur in two steps. The first step consists of a dislocation unbinding transition into an orientationally ordered liquid (hexatic phase). At higher temperatures there is a transition to an ordinary liquid phase. This picture is consistent with the notion that true long-range order is absent in two-dimensional matter. The latter effect is due to long-wavelength fluctuations (Jancovici 1967) which convert diffraction peaks to power-law singularities.

The theory of hexatic phases is not convincing enough to allow a systematic description of our data (Aeppli and Bruinsma 1984). Instead, it seems appropriate to attempt an analysis of the classical correlation (Patterson) function. In § 3, we deduce its general character and calculate the corresponding intensity.

3. Correlation function

Since the x-ray scattering of $T > T_c$ forms continuous streaks along the reciprocal c^* axis (Samuelsen *et al* 1984, 1985), the intercalated layers are known to be mutually uncorrelated in the disordered phase. The pronounced broadening of scattered intensity shows that the in-plane correlation length is limited.

We shall be able to give a general explanation for the intensity profiles by means of a simple model for non-uniform ordering in two dimensions. The total correlation $p(\boldsymbol{r})$ can be visualised as a sum of partial distributions for anti-convoluted electron density, i.e.

$$p(\boldsymbol{r}) = \sum_i p_i(\boldsymbol{r}). \tag{1}$$

In order to conserve the sixfold symmetry of the scattering diagram the positional and orientational order must be invariant during a rotation of $\pi/3$. Hence, a two-dimensional hexagonal lattice is a natural reference configuration for $p(\boldsymbol{r})$. Furthermore, since we want a continuous transition towards liquid-like disorder, the possibility of having angular broadening must be included. We give each partial distribution a 'banana' shape through the use of the expression

$$p_i(\boldsymbol{r}) = a^{(i)}(r - r_i)b^{(i)}(\Phi). \tag{2}$$

The distances between the partial distributions and origin are denoted by r_i and correspond to inter-molecular lengths. Radial half-widths are determined by the shape of the $a^{(i)}$-functions.

An arbitrary 'lattice'-like pattern of sixfold symmetry can be constructed by systematically superposing concentric hexagons. Since we want a correlation function that

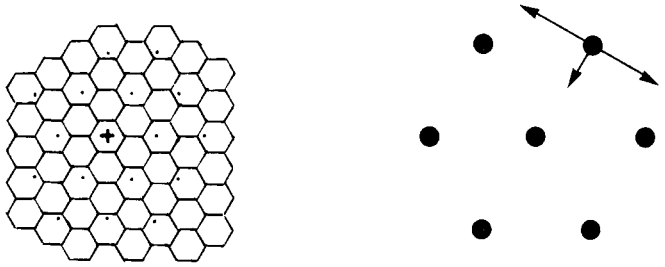

Figure 2. (*a*) Contracted hexagonal net (points). For convenience the net is shown superimposed on a graphite substrate (hexagons). The 'lattice' constant becomes progressively smaller as one moves away from the centre (+) towards the edge of the structure. (*b*) Displacement vectors. The vector directed towards the centre represents the effect of an inhomogeneous static deformation. The two transversally oriented vectors take care of the uncertainty in angular direction when the displacements are small.

tends to be non-zero in the vertex regions of the hexagons, their edge lengths are bound to be equal to r_i. A Fourier decomposition gives

$$p(\boldsymbol{r}) = \sum_i \sum_{\nu=0}^{n_i} a_\nu^{(i)}(r - r_i)\cos[6\nu(\Phi - \Phi_i)]. \tag{3}$$

The number n_i of harmonics for hexagon i determines the degree of azimuthal localisation. In order to fill the plane correctly, the various hexagons must have different rotational phases Φ_i with respect to the x axis.

Note that the following two features of the correlation function are indispensable.

(i) Near-neighbour distances between the distributions decrease as one moves away from the origin. This corresponds to a denser distribution of inter-molecular distances.

(ii) (i) is accompanied by a rapidly increasing azimuthal broadening.

The former effect (i) is equivalent to an inhomogeneous contraction of the hexagonal net and requires a new set of r_i values in (2). A varying angular broadening is accomplished by permitting the width of $b^{(i)}(\Phi)$ to be a function of r (figure 2(*b*)).

For completeness, we now give the intensity distribution. Fourier-transforming (3), we get

$$\tilde{p}(Q, \Psi) = \sum_i \sum_{\nu=0}^{n_i} \tilde{a}_\nu^{(i)}(Q)\cos[6\nu(\Psi - \Phi_i)] \tag{4}$$

where Ψ is the azimuthal angle of the scattering vector. Bessel functions of order 0, 6, 12, . . . determine the coefficients

$$\tilde{a}_\nu^{(i)}(Q) = (-1)^\nu \int r a_\nu^{(i)}(r) J_{6\nu}(Qr)\,\mathrm{d}r. \tag{5}$$

At high temperatures the double sums (3), (4) can be reduced to a few terms. Near T_c, however, the number of harmonics needed for a description of the angular localisation becomes unacceptably high. Nevertheless, it can be explicitly shown (Bremer *et al* 1988)

that the above picture of the correlation is capable of giving a general explanation for the peculiar broadening of the diffraction spots. This is done in the Appendix for small uncertainties in positional and orientational order.

4. Anchoring model

4.1. Model calculations

In this section, we introduce concrete molecular arrangements. The correlation function $p(\boldsymbol{r})$ will not be explicitly calculated but has to fall within the class discussed in § 3. The intensity is obtained through the relation $I(\boldsymbol{Q}) = |\tilde{\rho}(\boldsymbol{Q})|^2$ where $\tilde{\rho}(\boldsymbol{Q})$ is the Fourier transform of the actual distribution of average electron density.

The simplest possible choice for $p(\boldsymbol{r})$ is the correlation function of a truncated crystalline lattice. Experimentally, such a function is not easily distinguishable from the correlation function of an infinitely extended disordered structure. One important difference will be the absence of average long-range positional and orientational order. However, the main effect of the latter contribution is to increase the intensity at small scattering angles. In our measurements, intensity was not recorded below 5°.

We have worked out some numerical Fourier routines in order to study the effect of atomic displacements in small hexagonal domains. Each HNO_3 molecule has been replaced by a scattering centre consisting of a Gaussian two-dimensional electron density distribution. The radial density of each molecule goes as $\exp\{-\ln 2[(r - r_j)/\Gamma_1(r_j)]^2\}$. The r_j-values are given by the radial shifts whereas the radial uncertainty is taken care of by means of the parameter $\Gamma_1(r_j)$. For technical reasons the azimuthal distribution has been replaced by $\exp\{-\ln 2[y/\Gamma_2(r_j)]^2\}$ where $y \simeq r_j\theta$ is transverse with respect to $\boldsymbol{r}_j$. The origin is located at the centre of each cluster. A rapidly increasing angular uncertainty is allowed for by means of the parameter $\Gamma_2(r_j) \sim r_j^2$.

An essential part of our suggestion for the structure is that the clusters are anchored at fixed positions. The sixfold symmetry of the intensity shows that the allowed symmetries of these positions are either trigonal or hexagonal. Hence, both the centres and the vertices of the carbon hexagons are potential anchoring sites (figure 2(*a*)). The symmetries of these two anchoring possibilities are not modified by the graphite layers on the top of the nitrate molecules. The stacking sequence of graphite planes in stage 2 compounds is known to be $AB/BA/AB\ldots$, where a solidus (/) stands for an intercalant layer. The perpendicular antiferroelectric arrangement of HNO_3 molecules discussed by Touzain (1979) will likewise leave the symmetries unaffected. Note, however, that recently published infrared spectra (Conrad and Strauss 1985) together with nuclear resonance fluorescence data (Moreh *et al* 1986) do not exclude the possibility that the HNO_3 planes are weakly tilted with respect to the [001] direction of the graphite crystal.

The molecular structure factor has not been included in our calculations, since it would anyway involve only a slow dependence on the scattering vector. A similar assumption was made by Qian *et al* (1986) in a study of liquid layers in the ternary graphite intercalation compound $K(NH_3)_{4.33}C_{24}$. In their work, structure and diffraction pattern were modelled by means of computer-generated planar distributions of hard K^+ and NH_3 discs. The sizes of the NH_3 discs were permitted to vary according to a distribution function. In our recordings, we were unable to see second-order reflections. Hence, a substantial intensity reduction at high Q-values is believed to be the most conspicuous effect of the internal HNO_3 structure.

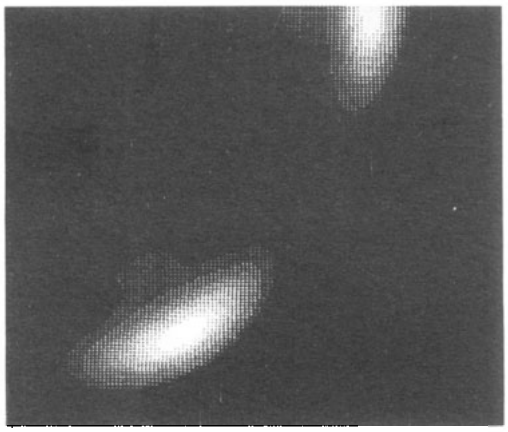

Figure 3. Effect of inhomogeneous radial contraction and angular uncertainty in a small two-dimensional crystal. The intensity pattern has six-fold symmetry and is rotated 30° with respect to the (100) reflections of graphite (see figure 2(*a*)). Distributions of this type result automatically when the radial contraction and the angular fluctuation of the molecules increase quadratically with increasing distance from the centre of the crystal. There is a range of parameters which are capable of qualitatively reproducing correct pictures. The domain giving the above intensity has an area of about 600 Å^2, containing 55 scattering centres. Although not essential for the effect, the radial widths are permitted to increase weakly with r according to $\Gamma_1(r) = 3 \times 10^{-2} r$ (Å). The radial and inhomogeneous contraction follows a $-1.3 \times 10^{-2} r^2$ law and the angular half-width goes as $\Gamma_2(r) = \Gamma_1(r) + 2.5 \times 10^{-2} r^2$.

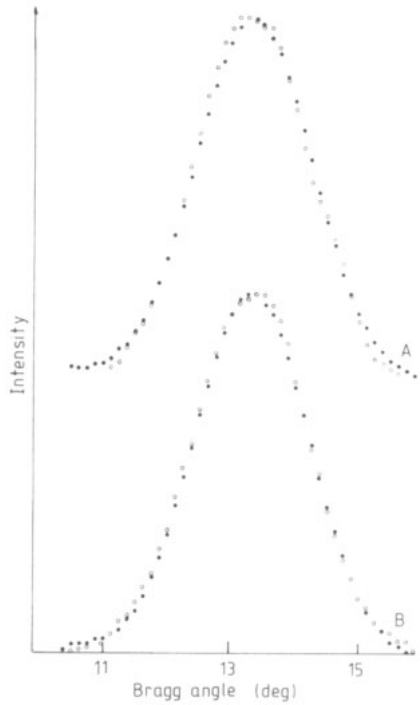

Figure 4. Intensity (curves A) as measured by a detector scan through an intensity maximum. Curves B show the intensity as a function of scattering angle at a reciprocal azimuthal angle of 5°. The model described in text (the anchoring model of § 4.2) gives fits shown by the full circles (curves A and B).

If we interpret figure 2(*a*) as a concrete structure (not a correlation function) the positions r_j of the depicted scattering centres will explain the rotation of 30° with respect to the graphite Bragg (100) reflections. With this lattice for the HNO_3 molecules, including the contractions, intensity distributions of the type shown in figure 3 are generated. The outer parts of the diffuse spots are seen to be strongly broadened in the azimuthal direction. It is found that the effect is achieved by allowing the angular Gaussian half-widths to increase rapidly with r in such a manner that Γ_2 is significantly larger than Γ_1.

4.2. Numerical results

We now show that our model is quantitatively reasonable, too. In general, at low temperatures, satisfactory fits to the experimental data have been obtained. As an example, we reproduce in figure 4 (curves A) a comparison between radially recorded (open circles) and calculated (full circles) intensities through one of six equivalent spots.

The small discrepancy is mostly due to the experimental uncertainty. Uncontracted, each cluster, of assumed circular shape, is found to have a diameter of 24 Å and to contain 37 molecules with an inter-molecular distance close to 4.0 Å. Such a value is incommensurate with the graphite structure; commensurability would require 4.26 Å = $a_G\sqrt{3}$.

At the edge of each cluster the quadratic lattice contraction is fitted to 0.9 Å. The average 'lattice' constant is thus effectively smaller than the nitrate–nitrate distance (about 4.0 Å) in solid HNO_3 (Luzzati 1951). It follows that the total out-of-phase step with respect to the carbon layers is 1.7 Å which is slightly longer than a graphite hexagon edge (1.4 Å). There is generally no easily recognisable relationship between the value for the shift and characteristic inter-atomic distances in graphite.

Furthermore, at different temperatures, new values for the fit parameters are found, and there is in addition a distribution of admissible cluster sizes and shapes. The average number of molecules in figure 4 is estimated to be somewhere between 40 and 50, whereas the cluster size variation is about 10–20%. The areas between the clusters are probably so disordered that scattered x-ray amplitudes from neighbouring islands have random phases.

Batallan *et al* (1988) have found evidence from inelastic neutron scattering for the translational motion of HNO_3 in the liquid phase, with jumps equal to 2.45 Å. This value is close to the in-plane lattice vector of graphite and shows that empty 'lattice gas' positions are available, possibly as a result of having locally commensurate regions. This type of disorder has been studied by Winokur *et al* (1982) who made numerical simulations of the structure factor corresponding to randomly decorated triangular lattices. It is interesting to note that such calculations in many cases can be performed analytically. Using two-dimensional Ornstein–Zernike relationships, it is possible to express the intensity pattern in terms of average vacancy concentration. The effect of imposing various exclusion distances (Bremer 1986) is easily taken care of through the choice of indirect correlation. The calculations, together with the experimental data, show that effects associated with lattice-gas disorder play a negligible role in HNO_3 GICs above 248 K.

The perturbing influence of a periodic host on alkali liquids has been discussed by Reiter and Moss (1986) and Moss *et al* (1986). The complex structural arrangement of HNO_3 in graphite is the outcome of competition between intercalant–host and intercalant–intercalant interaction. Because of polarisation and charge transfer effects the inter-molecular potential is rather different from the interaction in solid three-dimensional HNO_3. No signs of chain-like structures due to hydrogen bonds between the predominantly undissociated HNO_3 molecules have been found in this work.

5. Conclusions

We have reported a study of the x-ray scattering data for the intercalation compound $C_{10}HNO_3$. This two-stage compound has a series of complex phases. The characteristic features of the inter-molecular correlation function above 248 K are worked out. We believe that the observed diffraction pattern is due to local hexagonal orientational ordering which vanishes rapidly with increasing distance.

Specifically, at low temperatures a surprisingly simple realisation of the structure has been found. The model gives excellent fits to the experimental data. Briefly, it can be described as follows. Each second carbon layer contains inhomogeneously contracted

clusters. The clusters are relatively small and it is a very good approximation to assume that they scatter intensity independently of each other. The uncertainty in angular position increases rapidly while the HNO_3–HNO_3 distance becomes smaller as one moves from the centre to the edge of each cluster. This model represents a configurationally time-averaged approximation to the real structure.

Appendix

We now show that the proposed correlation function is capable of explaining the peculiar broadening in figure 1. It is convenient to define a reference configuration for the correlation function as

$$p_0(\boldsymbol{r}) = \sum_{j=1}^{\infty} \delta(\boldsymbol{r} - \boldsymbol{r}_j) T(\boldsymbol{r}) \tag{A1}$$

where $T(\boldsymbol{r})$ expresses the gradual correlation fall-off. We do not specify the exact shape at this stage since the most important effect of $T(\boldsymbol{r})$ is to broaden the diffraction spots. Note that the various $\boldsymbol{r}_j$-vectors specify a two-dimensional hexagonal lattice where $\boldsymbol{r}_j$ is the inter-molecular distance. Equation (A1) is thus applicable just above T_c where the degree of disorder is relatively small.

The correlation function (A1) consists of sharp Dirac functions. There are, crudely speaking, two qualitatively different ways of broadening $p_0(\boldsymbol{r})$. The various position-independent contributions can be included by simply convoluting (A1) with appropriate broadening functions. However, this results normally in a relatively slow $\boldsymbol{Q}$-dependence and will therefore not be included. In addition, however, there are anisotropic and non-uniform contributions, to be discussed below.

The lattice positions in (A1) are next shifted by a displacement field $\boldsymbol{d}(\boldsymbol{r})$. (Note that these shifts are introduced in order to study equation (1) just above T_c.)

$$p(\boldsymbol{r}) = \sum_{j=1}^{\infty} \delta[\boldsymbol{r} - \boldsymbol{r}_j - \boldsymbol{d}(\boldsymbol{r}_j)] T(\boldsymbol{r}). \tag{A2}$$

The Fourier transform of (A2) is

$$\tilde{p}(\boldsymbol{Q}) = \int \mathrm{d}\boldsymbol{r} \sum_{j=1}^{\infty} \delta(\boldsymbol{r} - \boldsymbol{r}_j) \exp\{\mathrm{i}\boldsymbol{Q} \cdot [\boldsymbol{r} + \boldsymbol{d}(\boldsymbol{r})]\} T(\boldsymbol{r}) \tag{A3}$$

which can be rewritten as

$$\tilde{p}(\boldsymbol{Q}) = \tilde{p}_0(\boldsymbol{Q}) + \int \mathrm{d}\boldsymbol{r} \sum_{j=1}^{\infty} T(\boldsymbol{r}) \delta(\boldsymbol{r} - \boldsymbol{r}_j) \exp(\mathrm{i}\boldsymbol{Q} \cdot \boldsymbol{r}) \{\exp[\mathrm{i}\boldsymbol{Q} \cdot \boldsymbol{d}(\boldsymbol{r})] - 1\}. \tag{A4}$$

Using $I = \langle \tilde{p}(\boldsymbol{Q}) \rangle$ and expanding the exponential function inside the parentheses, we find for the intensity

$$I = \tilde{p}_0 + \int \mathrm{d}\boldsymbol{r} \sum_{j=1}^{\infty} T(\boldsymbol{r}) \delta(\boldsymbol{r} - \boldsymbol{r}_j) \exp(\mathrm{i}\boldsymbol{Q} \cdot \boldsymbol{r}) \langle \{\mathrm{i}\boldsymbol{Q} \cdot \boldsymbol{d}(\boldsymbol{r}) - \tfrac{1}{2}[\boldsymbol{Q} \cdot \boldsymbol{d}(\boldsymbol{r})]^2 + \ldots\} \rangle. \tag{A5}$$

The averaging operation refers to a configurational average and such processes as diffusion jumps and vibrational motion.

We now split $\boldsymbol{d}$ into two parts:

$$\boldsymbol{d}(\boldsymbol{r}) = \boldsymbol{U}(\boldsymbol{r}) + \boldsymbol{u}(\boldsymbol{r}). \tag{A6}$$

The first term expresses a static deformation whereas the second term is due to time-

dependent fluctuations. The intensity can be written as

$$I = \tilde{p}_0 + S_1 + S_2 + S_3 + \dots \tag{A7}$$

where $S_1, S_2, \dots$ will be discussed below. We shall utilise the facts that $\langle \boldsymbol{u} \rangle = \boldsymbol{0}$ while $\langle \boldsymbol{U} \rangle$, $\langle \boldsymbol{U}^2 \rangle$ and $\langle \boldsymbol{u}^2 \rangle$ are non-zero. A truncation is possible after the first few terms in (A7) when $\langle \boldsymbol{Q} \cdot \boldsymbol{d} \rangle \ll 1$. This is a valid approximation if $T(\boldsymbol{r})$ goes to zero sufficiently rapidly.

We also note that an expansion of the shift $\boldsymbol{d}(\boldsymbol{r})$ can start with the second-order term $|\boldsymbol{d}| \sim r^2$ when $\boldsymbol{U}(\boldsymbol{r})$ is isotropic and radial, i.e. $\boldsymbol{U}(\boldsymbol{r}) = U(r)\hat{\boldsymbol{e}}_1$. The reason is that linear terms $U \sim \pm r$ correspond to a homogeneous dilation or contraction of the lattice and this amounts only to a redefinition of the lattice constant, the effect of which can be absorbed into the definition of $p_0(\boldsymbol{r})$ as given by equation (A1). (In the case of HNO_3 in graphite the radial shift is found to be negative.) The directions of $\boldsymbol{U}(\boldsymbol{r})$ and $\boldsymbol{u}$ are shown in figure 2(*b*). It can be shown (Bremer 1986) that components of $\boldsymbol{U}(\boldsymbol{r})$ along $\hat{\boldsymbol{e}}_2$ entail azimuthally oriented and symmetrically located satellite peaks. Such effects have not been observed in our experiments and are henceforth neglected.

Defining

$$\tilde{U}(\boldsymbol{Q}) = 2\pi \int_0^\infty r|U|T(r)J_1(Qr)\,\mathrm{d}r\,\hat{\boldsymbol{e}}_1 \tag{A8}$$

after making the reasonable assumption that $T = T(|\boldsymbol{r}|)$, we obtain

$$S_1(\boldsymbol{Q}) = \boldsymbol{Q} \sum_n \delta(\boldsymbol{Q} - \boldsymbol{Q}_n) \otimes \tilde{U}(\boldsymbol{Q}) \tag{A9}$$

i.e. the transform of the (vectorial) displacement field $\tilde{\boldsymbol{U}}(\boldsymbol{Q})$ is distributed at the reciprocal lattice points $\boldsymbol{Q}_n$ by means of a folding operation. Equation (9) generates an intensity pattern with sixfold symmetry. Concentrating on the hexagonally distributed points nearest the origin, and referring $\boldsymbol{Q}$ to one of the six equivalent lattice points Q_1, $\boldsymbol{Q}' = \boldsymbol{Q} - \boldsymbol{Q}_1$, we get

$$S_1(Q') = \tilde{U}(Q')(Q' + Q_1 \cos\psi) \tag{A10}$$

where ψ is the angle between $\boldsymbol{Q}'$ and $\boldsymbol{Q}_1$. Hence, the intensity is transferred from that part of the broadened spot which is closest to the origin. The intensity is shifted outwards and the profile becomes asymmetric.

We now assume that $\langle u^2 \rangle \gg \langle U^2 \rangle$, i.e. the second-order term S_3 from the static displacement is neglected. The rationale for this choice is the wish to keep the model as simple as possible. Defining

$$\tilde{a}(Q') = \pi \int \mathrm{d}r\, r\langle u^2 \rangle T(r) J_2(Q'r) \tag{A11}$$

$$\tilde{b}(Q') = \pi \int \mathrm{d}r\, r\langle u^2 \rangle T(r) \frac{J_1(Q'r)}{Q'r} \tag{A12}$$

we find after some calculations that

$$S_2 = Q^2\{\tilde{p}_0 \otimes [\tilde{a}\sin^2(\Psi - \psi) - \tilde{b}]\}. \tag{A13}$$

The angle between $\boldsymbol{Q}$ and $\boldsymbol{Q}_n$, denoted by Ψ, is of order Q'/Q_1 which is much smaller than unity at low temperatures.

The above equation (A13) describes two azimuthally oriented side lobes. In agreement with the experimental observations the combined effect of (A9) and (A12) is to increase the intensity at the outside of the spots and to 'stretch' them along the angular direction. At higher temperatures, we get a gradual development of a modulated ring.

References

Aeppli G and Bruinsma R 1984 *Phys. Rev. Lett.* **53** 2133–6
Batallan F, Rosenman I and Simon C 1988 *Synth. Met.* **23** 49–53
Bremer J 1986 unpublished
Bremer J, Samuelsen E and Moret R 1988 *Z. Kristallogr.* **185** 527
Conrad M P and Strauss H L 1985 *Phys. Rev.* B **31** 6669–75
Fuzellier H, Melin J and Hérold A 1977 *Mater. Sci. Eng.* **31** 91–6
Halperin B I and Nelson D R 1978 *Phys. Rev. Lett.* **41** 121–4
Jancovici B 1967 *Phys. Rev. Lett.* **19** 20–2
Lundberg B and Sundqvist B 1986 *Solid State Commun.* **58** 747–51
Luzzati V 1951 *Acta Crystallogr.* **4** 120–31
Moreh R, Shakal O and Kimmel G 1986 *Phys. Rev.* B **33** 5717–20
Moss S C, Reiter G, Robertson J L, Thompson C and Fan J D 1986 *Phys. Rev. Lett.* **57** 3191–4
Qian X W, Stump D R and Solin S A 1986 *Phys. Rev.* B **33** 5756–69
Reiter G and Moss S C 1986 *Phys. Rev.* B **33** 7209–17
Samuelsen E J, Moret R, Comès R, Fuzellier H, Klatt M, Lelaurin M and Hérold A 1984 *Synth. Met.* **10** 13–9
Samuelson E J, Moret R, Fuzellier H, Klatt M, Lelaurin M and Hérold A *Phys. Rev.* B **31** 417–27
Samuelsen E J, Moret R and Høier R 1987 *J. Phys. E: Sci. Instrum.* **20** 1264–8
Touzain P 1979 *Synth. Met.* **1** 3–11
Winokur M J, Rose J H and Clarke R 1982 *Phys. Rev.* B **25** 3703–13